Dissociation products and structures of solid H_2S at strong compression

Supplementary Material

Yinwei Li,[1] Lin Wang,[2,3] Hanyu Liu,[3,4] Yunwei Zhang,[3] Jian Hao,[1] Chris J. Pickard,[5] Joseph R. Nelson,[6] Richard J. Needs,[6] Wentao Li,[2] Yanwei Huang,[2] Ion Errea,[7,8] Matteo Calandra,[9] Francesco Mauri,[9] and Yanming Ma[3*]

[1]*School of Physics and Electronic Engineering, Jiangsu Normal University, Xuzhou 221116, P. R. China*
[2]*Center for High Pressure Science and Technology Advanced Research, Shanghai, 201203, P. R. China*
[3]*State Key Laboratory of Superhard Materials, Jilin University, Changchun 130012, P. R. China*
[4]*Geophysical Laboratory, Carnegie Institution of Washington, Washington D.C. 20015, USA*
[5]*Department of Materials Science & Metallurgy, University of Cambridge, 27 Charles Babbage Road, Cambridge CB3 0FS, United Kingdom*
[6]*Theory of Condensed Matter Group, Cavendish Laboratory, J J Thomson Avenue, Cambridge CB3 0HE, United Kingdom*
[7]*Donostia International Physics Center (DIPC), Manuel de Lardizabal pasealekua 4, 20018 Donostia-San Sebastián, Basque Country, Spain*
[8] *Fisika Aplikatua 1 Saila, EUITI Bilbao, University of the Basque Country (UPV/EHU), Rafael Moreno "Pitxitxi" Pasealekua 3, 48013 Bilbao, Basque Country, Spain*
[9]*IMPMC, UMR CNRS 7590, Sorbonne Universités - UPMC Univ. Paris 06, MNHN, IRD, 4 Place Jussieu, F-75005 Paris, France*

Correspondence and requests for materials should be addressed to Y. Ma (mym@jlu.edu.cn).

Computational and experimental details

Extensive structure searches were performed at 25, 50, 100 and 150 GPa with a maximum of eight formula units (f.u.) in the simulation cell for each stoichiometry considered. 44 H-S stoichiometries (H_2S_3, H_4S, HS_3, H_4S_3, HS_4, H_2S, HS_2, H_8S_3, S, HS, H, H_7S_4, H_8S_5, HS_6, H_3S_7, H_7S_3, H_3S_4, H_3S_5, HS_5, H_5S, H_3S, H_6S, H_8S_7, H_7S, H_8S, H_3S_8, H_5S_2, H_5S_3, H_5S_8, HS_7, H_5S_4, H_2S_7, H_7S_5, H_6S_5, H_7S_2, HS_8, H_4S_5, H_7S_6, H_2S_5, H_7S_8, H_5S_7, H_6S_7, H_3S_2, H_9S_2) were considered in the structure searches, which were performed using the efficient CALYPSO and AIRSS methods. In the structure predictions, the underlying *ab initio* structure relaxations were performed using the Vienna *ab initio* simulation package (VASP) for CALYPSO and the CASTEP plane-wave code for AIRSS. The Perdew-Burke-Ernzerhof generalized gradient approximation was used to treat electron exchange/correlation, and the all-electron projector augmented wave method was adopted in VASP calculations, while ultrasoft pseudopotentials were used for the CASTEP calculations. For the structure searches, a plane-wave cutoff energy of 700 eV and a Brillouin zone integration grid spacing of $2\pi \times 0.05$ Å^{-1} was used. The structures obtained were reoptimized using the VASP code at a higher level of accuracy with grids denser than $2\pi \times 0.03$ Å^{-1} and a cutoff energy of 1000 eV, resulting in convergence of the total energy to better than 1 meV/atom. Electron-phonon coupling (EPC) calculations were performed with density functional perturbation theory using the Quantum-ESPRESSO package with a kinetic energy cutoff of 90 Ry. A 4×4×3 *q*-point mesh in the first Brillouin zone was used in the EPC calculations. A MP grid of 8×8×6 was used to ensure *k*-point sampling convergence with Gaussians of width 0.03 Ry, which approximates the zero-width limits in the calculations of the EPC parameter λ.

A symmetric type diamond anvil cell with beveled culets of 150 μ*m* was used to generate high pressures. H_2S of 99.99% purity was solidified with a cryogenic method and loaded into a 70 μm hole drilled in a Tungsten gasket. We firstly cool the open DAC down to ~77K, then let pure H_2S flow through the sample chamber and the gas directly solidified when it reached the diamonds and gasket. The DAC was closed with an initial pressure of 10 GPa and warmed up to room temperature. All other pressure points were measured at room temperature. The pressure was measured by the shift of the Raman peak of diamond excited by a 532 nm laser. The X-ray diffraction (XRD) patterns were collected at the 15U1 beamline at the Shanghai Synchrotron Radiation Facility (SSRF) using a MAR345 flat panel detector at room temperature. A monochromatic beam of 0.6199 Å was used. The diffraction patterns were integrated with the FIT2D computer code. High-pressure synchrotron X-ray patterns were fitted by Rietveld profile matching using the *GSAS+EXPGUI* programs. During each refinement cycle, the fractional coordinates, scale factor, background parameter, isotropic thermal parameters, profile function, and cell parameter were optimized.

TABLE S1. Crystallographic data for H_4S_3 at 25 and 100 GPa obtained from structure searches. At 50 GPa, H_4S_3 adopts the same $P2_12_12_1$ structure as at 25 GPa. At 150 GPa, H_4S_3 adopts the same Pnma structure as at 100 GPa.

Space group	Pressure (GPa)	Lattice parameters (Å, deg.)	Atomic coordinates (fractional)
$P2_12_12_1$	25	*a* = 6.1274 *b* = 7.1916 *c* = 5.3034	S1 (4*a*) (0.9276, 0.6737, 1.5007) S2 (4*a*) (0.0804, 0.5105, 1.0121) S3 (4*a*) (0.1097, 0.8417, 1.0015) H1 (4*a*) (0.7727, 0.6710, 1.3099) H2 (4*a*) (0.2901, 0.4978, 1.2961) H3 (4*a*) (0.1109, 0.3469, 1.5103) H4 (4*a*) (0.2298, 0.1719, 0.8104)
Pnma	100	*a* = 5.2748 *b* = 4.5891 *c* = 6.6816	S1 (4*c*) (0.2156, 0.25, 0.3120) S2 (4*c*) (0.3089, 0.75, 0.4967) S3 (4*c*) (0.3598, 0.75, 0.1238) H1 (8*d*) (0.0298, 0.0345, 0.3107) H2 (4*c*) (0.3892, 0.25, 0.6748) H3 (4*a*) (0, 0, 0)

TABLE S2. Crystallographic data for H_2S_3 and H_3S_2 at 25 GPa and HS_2 at 100 GPa obtained from structure searches. At 25 GPa, H_2S_3 adopts the C2 structure and H_3S_2 has two energetically nearly identical structures with space groups Cm and P1. At 100 GPa, HS_2 has a tetragonal P4/nmm structure.

Compounds	Space group	Lattice parameters (Å, deg.)	Atomic coordinates (fractional)
H_2S_3	C2	a = 5.5789 b = 3.4282 c = 6.1113 β = 117.697	S1 (4*c*) (0.6183, -0.4907, 0.2995) S2 (2*a*) (0, -0.6187, 0) H (4*c*) (0.1224, -0.5215, 0.662)
H_3S_2	Cm	a = 9.542 b = 5.1579 c = 3.3564 β = 117.697	S1(2*a*) (-0.4677, -0.5, 0.6173) S2(2*a*) (-0.1702, -0.5, 0.3027) S3(2*a*) (0.2565, -0.5, 0.8214) S4(2*a*) (0.0713, -0.5, 0.0273) H1(4*b*) (-0.2066, -0.2973, 0.5483) H2(4*b*) (0.0603, -0.2016, 0.3609) H3(2*a*) (-0.3055, -0.5, 0.0059) H4(2*a*) (0.3596, -0.5, 0.1851)
H_3S_2	P1	a = 5.4099 b = 5.8747 c = 6.2578 α = 98.309 β = 108.755 γ = 113.33	S1 (1a)(0.8872, 0.9325, 0.8788) S2 (1a)(0.4156, 0.4699, 0.3921) S3 (1a)(0.7835, 0.9751, 0.3231) S4 (1a)(0.2807, 0.9571, 0.1179) S5 (1a)(0.2795, 0.4246, 0.8204) S6 (1a)(0.7772, 0.4283, 0.5865) S7 (1a)(0.3407, 0.9702, 0.6123) S8 (1a)(0.8856, 0.4650, 0.1514) H1 (1a)(0.5396, 0.6489, 0.8734) H2 (1a)(0.4265, 0.9859, 0.8447) H3 (1a)(0.9812, 0.6664, 0.5832) H4 (1a)(0.8063, 0.7512, 0.2529) H5 (1a)(0.9278, 0.1642, 0.0142) H6 (1a)(0.1924, 0.2482, 0.3979) H7 (1a)(0.3433, 0.4415, 0.0562) H8 (1a)(0.2315, 0.7292, 0.9705) H9 (1a)(0.8201, 0.9654, 0.5485) H10 (1a)(0.6156, 0.2604, 0.1055) H11 (1a)(0.8122, 0.4566, 0.9151) H12 (1a)(0.3908, 0.7622, 0.5509)
HS_2	P4/nmm	a = 3.0815 c = 4.7827	S1 (2*a*) (0, 0, 0) S2 (2*c*) (0, 0.5, 0.45961) H (2*c*) (0.5, 0, 0.26189)

TABLE S3. Crystallographic data for H_3S at 25 GPa obtained from structure searches. At 50 and 100 GPa, H_3S adopts the same C2/c structure as at 25 GPa.

Space group	Pressure (GPa)	Lattice parameters (Å, deg.)	Atomic coordinates (fractional)
C2/c	25	a = 8.9559 b = 5.2145 c = 9.9831 β = 117.53	S1 (8*f*) (-0.9117, 0.3670,-0.0866) S2 (8*f*) (-0.8327, 0.1349, 0.2561) H1 (8*f*) (-1.0796, 0.1489,-0.0005) H2 (8*f*) (-1.1612, 0.1084,-0.0030) H3 (8*f*) (-0.8192, 0.4749, 0.0579) H4 (8*f*) (-1.0703, 0.0712,-0.1805) H5 (8*f*) (-0.7346, 0.1197, 0.1801) H6 (8*f*) (-0.9883, 0.4181, 0.1482)

TABLE S4. Rietveld refined structure parameters of H_2S-Pc, H_4S_3-$P2_12_12_1$, H_3S-C2/c and S-$I4_1$/acd at 45.6 GPa.

Compounds	Lattice parameters (Å, deg.)	Atomic coordinates (fractional)
H_2S-Pc	*a* = 5.2995 *b* = 3.05095 *c* = 4.9354 *β* = 77.8994	S1 (2*a*) (0.0011, 0.18816, 0.63515) S2 (2*a*) (0.49733, 0.35482,0.34277) H1 (2*a*) (0.76754, 0.07442, 0.20676) H2 (2*a*) (0.26261, 0.86819, 0.73009) H3 (2*a*) (0.98632, 0.43407, 0.85914) H4 (2*a*) (0.5002, 0.05799, 0.53346)
H_4S_3-$P2_12_12_1$	*a* = 5.805900 *b* = 7.172200 *c* = 5.003000	S1 (4*a*) (0.44463, 0.69593, 0.99991) S2 (4*a*) (0.57637, 0.49679, 0.50734) S3 (4*a*) (0.62305, 0.87449, 0.50128) H1 (4*a*) (0.27982, 0.68229, 0.78963) H2 (4*a*) (0.76955, 0.49876, 0.77504) H3 (4*a*) (0.60337, 0.3232, 1.00264) H3 (4*a*) (0.72166, 0.18402, 1.28889)
H_3S-C2/c	*a* = 8.41678 *b* = 4.9844 *c* = 15.2985 *β* = 146.3395	S1 (8*f*) (1.25589, 0.13361, -0.41663) S2 (8*f*) (1.15919, -0.13735, 0.24572) H1 (8*f*) (0.92122, 0.35125, 0.49914) H2 (8*f*) (1.34064, -0.11114, -0.49827) H3 (8*f*) (1.05094, 0.00928, 0.42838) H4 (8*f*) (0.79196, -0.0813, -0.32179) H5 (8*f*) (0.93032, 0.37845, 0.32638) H6 (8*f*) (0.71116, 0.08964, 0.34626)
S-$I4_1$/acd	*a* = 8.045500 *c* = 3.233600	S (16*f*)(0.63282, -0.13282, -0.50000)

TABLE S5. Rietveld refined structure parameters of H_4S_3-Pnma, H_3S-C2/c and H_2S-Pc at 65.7 GPa.

Compounds	Lattice parameters (Å, deg.)	Atomic coordinates (fractional)
H_4S_3-Pnma	*a* = 5.553044 *b* = 4.841780 *c* = 6.892122	S1 (4*c*) (0.20446,0.75,0.30774) S2 (4*c*) (0.36627,0.25,0.12373) S3 (4*c*) (0.32036,0.25,0.49864) H1 (8*d*) (0.03174,0.53769,0.31406) H2 (4*c*) (0.36974,0.75,0.67366) H3 (4*a*) (0.5,0.5, 0.5)
H_3S-C2/c	*a* = 8.116226 *b* = 4.823228 *c* = 14.222078 *β* = 146.2886	S1 (8*f*) (-0.24926,-0.36275,-0.58061) S2 (8*f*) (0.33849,-0.14017,-0.24731) H1 (8*f*) (0.08186,-0.14749,-0.49649) H2 (8*f*) (0.15934,-0.11349,-0.5036) H3 (8*f*) (-0.04062,-0.50181,-0.42009) H4 (8*f*) (-0.29244,-0.08966,-0.67534) H5 (8*f*) (0.05369,-0.1255,-0.3301) H6 (8*f*) (0.29395,-0.40798,-0.3403)
H_2S-Pc	*a* = 4.756800 *b* = 2.976300 *c* = 5.013700 *β* = 90.0612	S1 (2*a*) (0.96954, 0.86851, 0.11639) S2 (2*a*) (0.47009, 0.68204, 0.84172) H1 (2*a*) (0.71972, 0.38379, 0.75170) H2 (2*a*) (-0.03079, 0.44762, 0.42335) H3 (2*a*) (0.46823, 0.05161, 0.1097) H4 (2*a*) (0.2215, 0.61181, 0.25379)

TABLE S6. Rietveld refined structure parameters of H_4S_3-Pnma, H_3S-C2/c and H_2S-Pmc2_1 at 81.3 GPa.

Compounds	Lattice parameters (Å, deg.)	Atomic coordinates (fractional)
H_4S_3-Pnma	*a* = 5.454762 *b* = 4.757546 *c* = 6.710423	S1 (4*c*) (0.21213, 0.25, 0.32810) S2 (4*c*) (0.32425, 0.75, 0.50068) S3 (4*c*) (0.36113, 0.75, 0.11033) H1 (8*d*) (0.02458, 0.03966, 0.33951) H2 (4*c*) (0.40858, 0.25, 0.47521) H3 (4*a*) (0.5,0.5, 0.5)
H_3S-C2/c	*a* = 8.3854 *b* = 4.7027 *c* = 14.9809 *β* = 147.0144	S1 (8*f*) (-0.24493, -0.35806, -0.57868) S2 (8*f*) (0.31931, -0.16206, -0.255) H1 (8*f*) (0.09096, -0.14921, -0.49182) H2 (8*f*) (0.15254, -0.11522, -0.50989) H3 (8*f*) (-0.03898, -0.50574, -0.41760) H4 (8*f*) (-0.28955, -0.09033, -0.67268) H5 (8*f*) (0.05165, -0.13138, -0.32918) H6 (8*f*) (0.29572, -0.41143, -0.33793)
H_2S-Pmc2_1	*a* = 4.7433 *b* = 3.0061 *c* = 4.9109	S1 (2*a*) (0, 0.1766, 0.61978) S2 (2*b*) (-0.5, 0.37912, 0.35749) H1 (4*c*) (-0.24957, 1.12283, 0.21273) H2 (2*a*) (0, 0.44805, 0.85499) H3 (2*b*) (-0.5, 1.05136, 0.54966)

TABLE S7. Rietveld refined structure parameters of H_4S_3-Pnma, H_3S-R3m and H_2S-P-1 at 139.5 GPa.

Compounds	Lattice parameters (Å, deg.)	Atomic coordinates (fractional)
H_4S_3-Pnma	*a* = 5.100185 *b* = 4.544369 *c* = 6.434815	S1 (4*c*) (0.82227, 0.25, 0.50816) S2 (4*c*) (0.72131, 0.75, 0.41929) S3 (4*c*) (0.71448, 0.75, 0.69670) H1 (8*d*) (0.97604, 0.03629, 0.80906) H2 (4*c*) (0.94095, 0.75, 0.64608) H3 (4*b*) (0.5, 0, 0)
H_3S-R3m	*a* = 4.4292 *c* = 2.7147	S (3*a*) (0, 0, 0.11341) H (9*b*) (-0.30002, -0.15001, 0.42488)
H_2S-P-1	*a* = 2.6704 *b* = 2.6833 *c* = 4.1109 α =102.98 β = 76.618 γ =110.358	S1 (2*i*) (0.31229,0.18158,0.23858) H1 (2*i*) (0.1966,0.37478,0.82988) H2 (1*g*) (0.000, 0.500, 0.500) H3 (1*f*) (0.500, 0.000, 0.500)

TABLE S8. The calculated logarithmic average of the phonon frequency (ω_{log}), EPC parameter (λ), and critical temperature T_c (μ^* = 0.13, 0.16) of Pnma-H_4S_3. The superconducting T_c was estimated using the Allen and Dynes modified McMillan equation.

Phases	P (GPa)	λ	ω_{log} (K)	T_c (K)	
				μ^* = 0.13	μ^* = 0.16
Pnma-H_4S_3	140	0.42	834	2.1	0.75

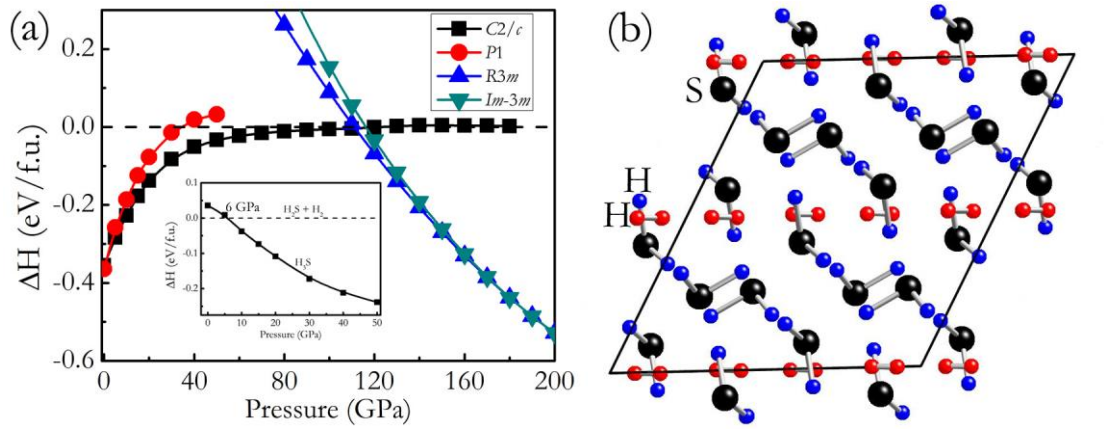

Fig. S1. (a) Calculated enthalpy curves for various structures of H_3S relative to the previously predicted Cccm structure as a function of pressure. The inset in (a) represents the enthalpy of H_3S relative to H_2S and H_2. (b) The C2/c structure predicted for H_3S at 25, 50 and 100 GPa consists of well separated H_2S and H_2 molecules.

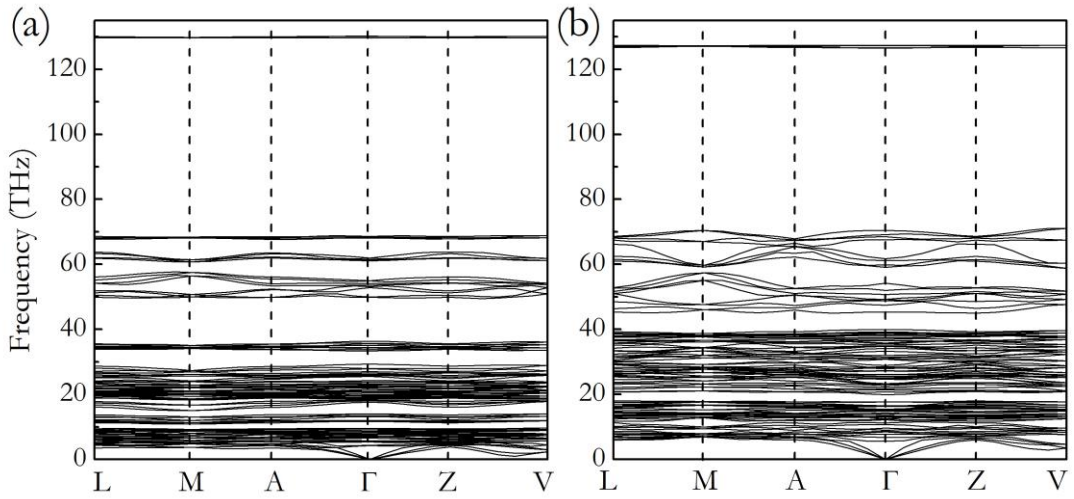

Fig. S2. Calculated phonon dispersion curves of the C2/c structure for H_3S at 25 (a) and 100 GPa (a). No any imaginary phonons were found within the corresponding stable pressures ranges, demonstrating the dynamical stability of the structure.

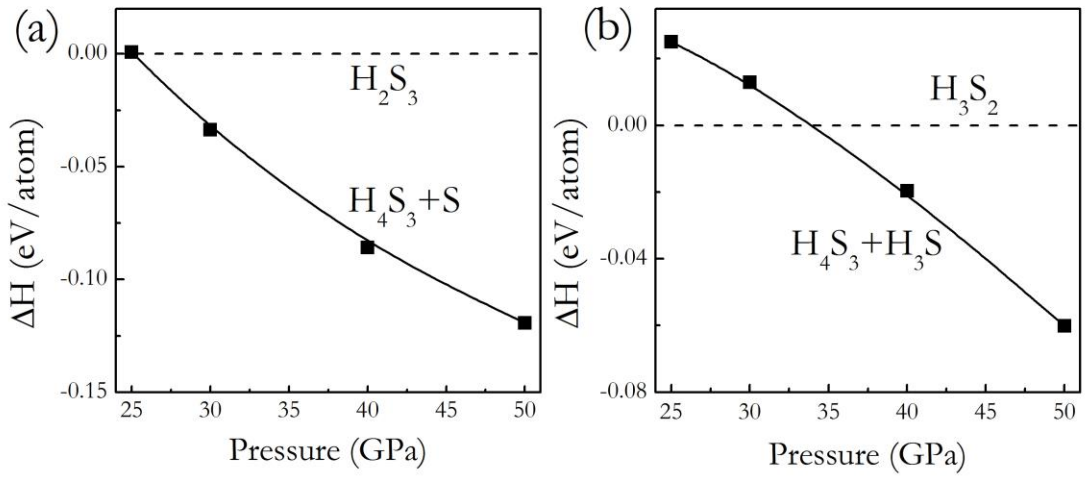

Fig. S3. (a) Decomposition enthalpy curves of H_2S_3 into H_4S_3+S, and (b) of H_3S_2 into H_4S_3+H_3S, as functions of pressure. H_2S_3 is unstable above 25 GPa, and H_3S_2 is unstable above 34 GPa.

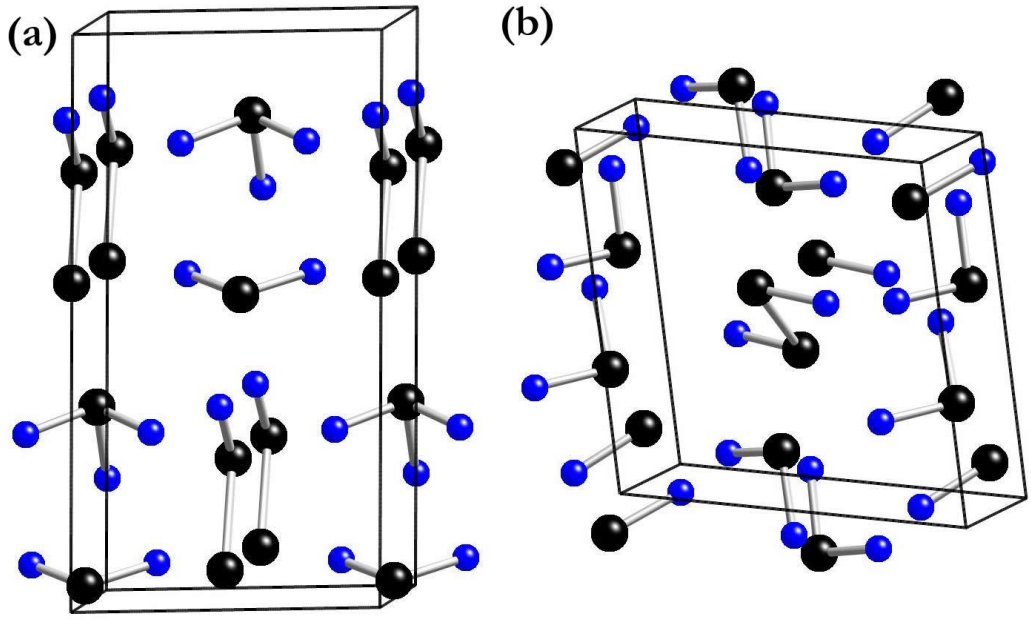

Fig. S4. Predicted crystal structures of H_3S_2 with space groups Cm (a) and P1 (b). Large black and small blue spheres represent S and H atoms, respectively. The Cm structure consists of H_3S, H_2S and HS_2 molecules and the P1 structure consists of H_2S_2 and H_2S molecules.

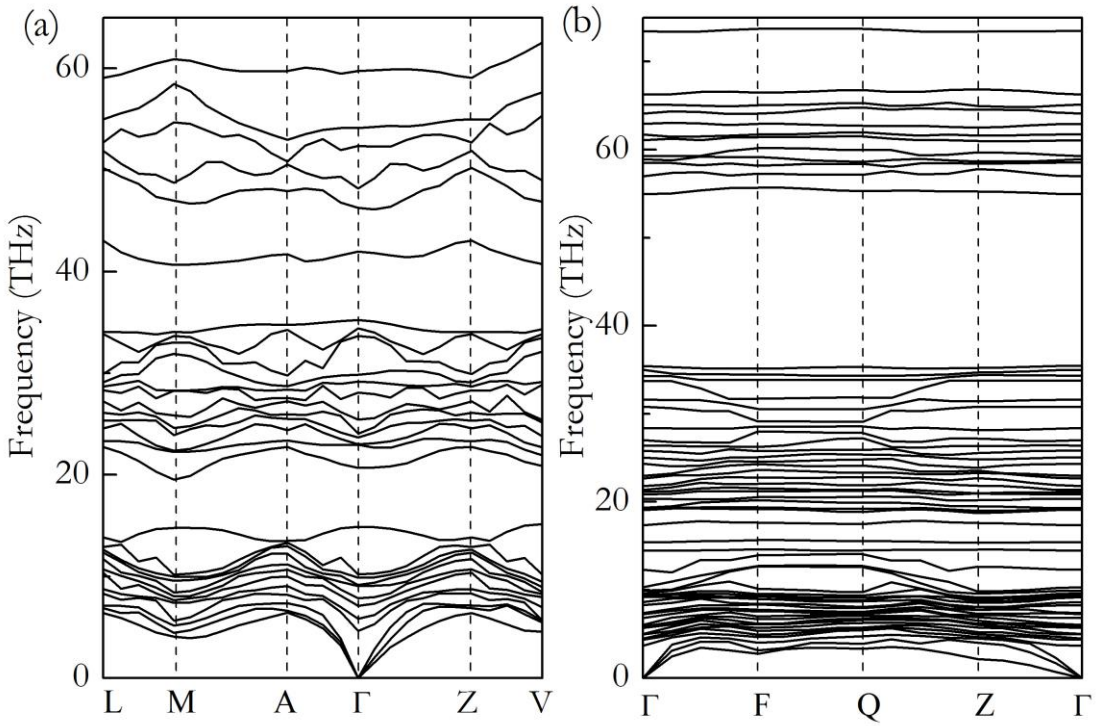

Fig. S5. Calculated phonon dispersion curves of the Cm structure (a) and the P1 structure (b) for H_3S_2 at 25 GPa. No any imaginary phonons were found, demonstrating the dynamical stability of the two structures.

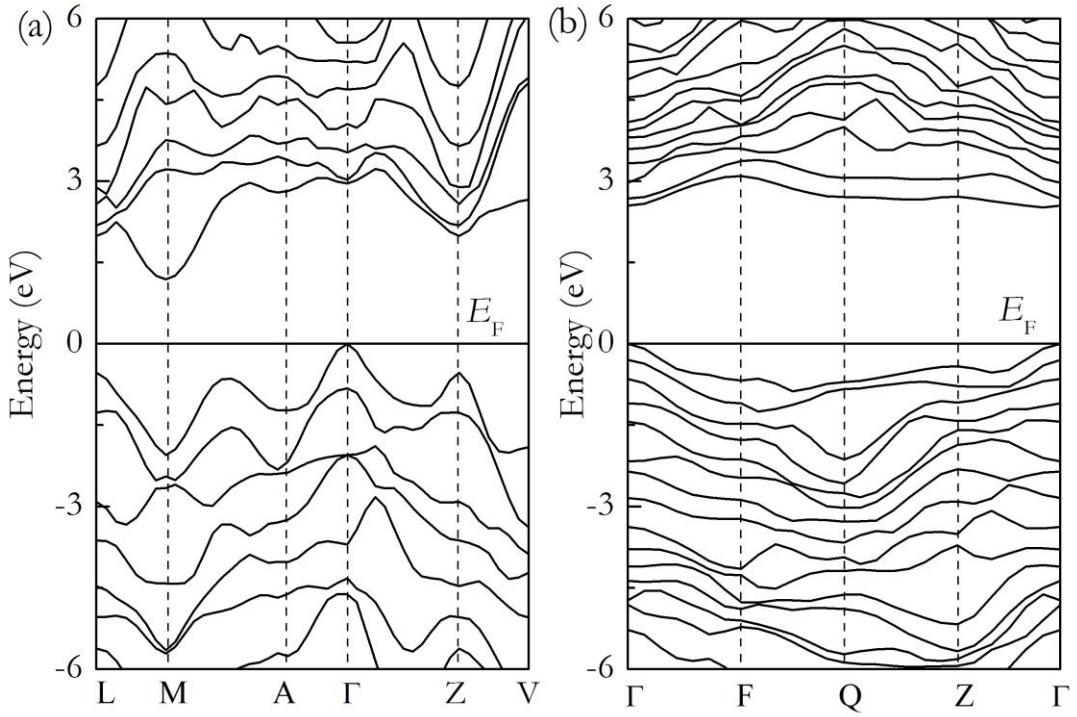

Fig. S6. Electronic band structures of the Cm (a) and the P1 (b) structures of H_3S_2 at 25 GPa. The band gaps of the Cm and the P1 structures calculated using the PBE-GGA functional are 1.2 eV and 2.5 eV, respectively.

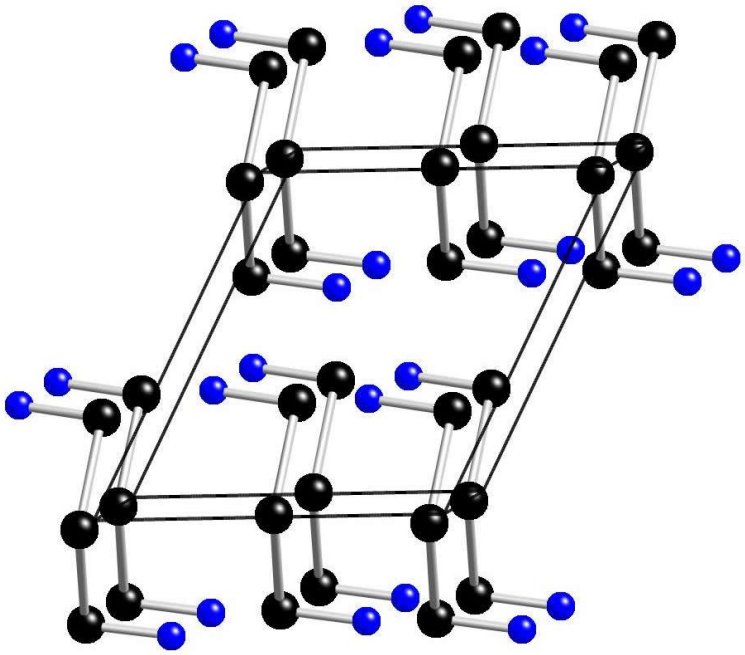

Fig. S7. Crystal structure of H_2S_3 with space group C2. Large black and small blue spheres represent S and H atoms, respectively. The C2 structure is constructed from H_2S_3 molecules.

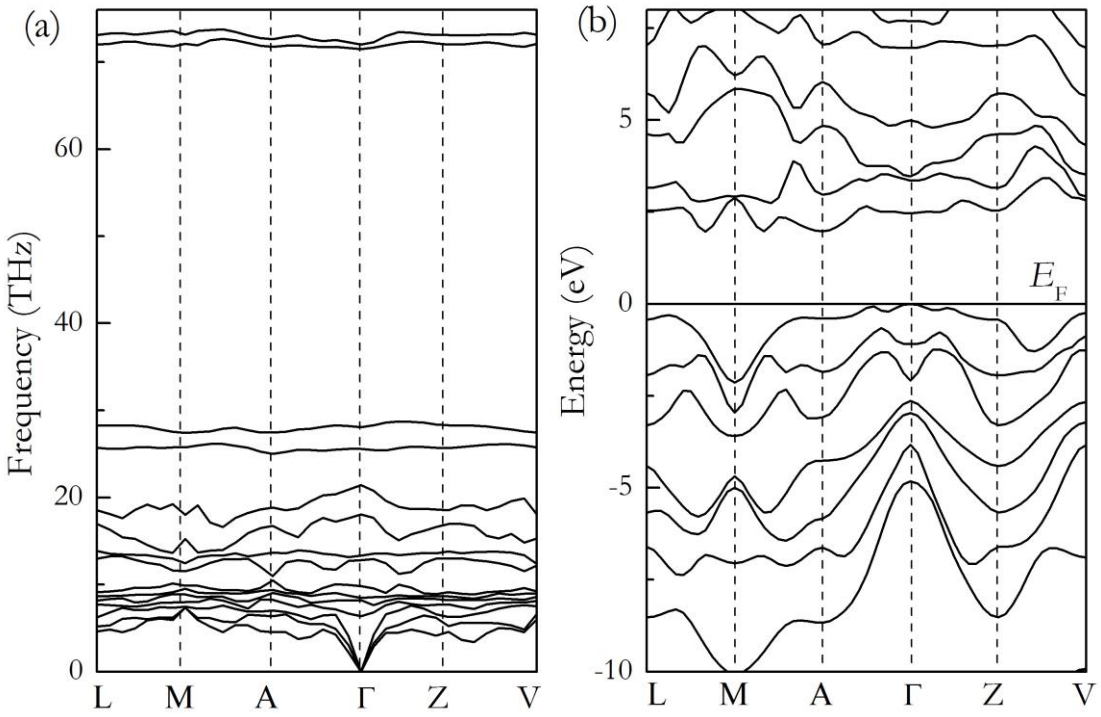

Fig. S8. Calculated phonon dispersion curves (a) and electronic band structure (b) of the C2 structure of H_2S_3 at 25 GPa. The C2 structure is dynamically stable and is a semiconductor with a band gap of 1.9 eV at 25 GPa .

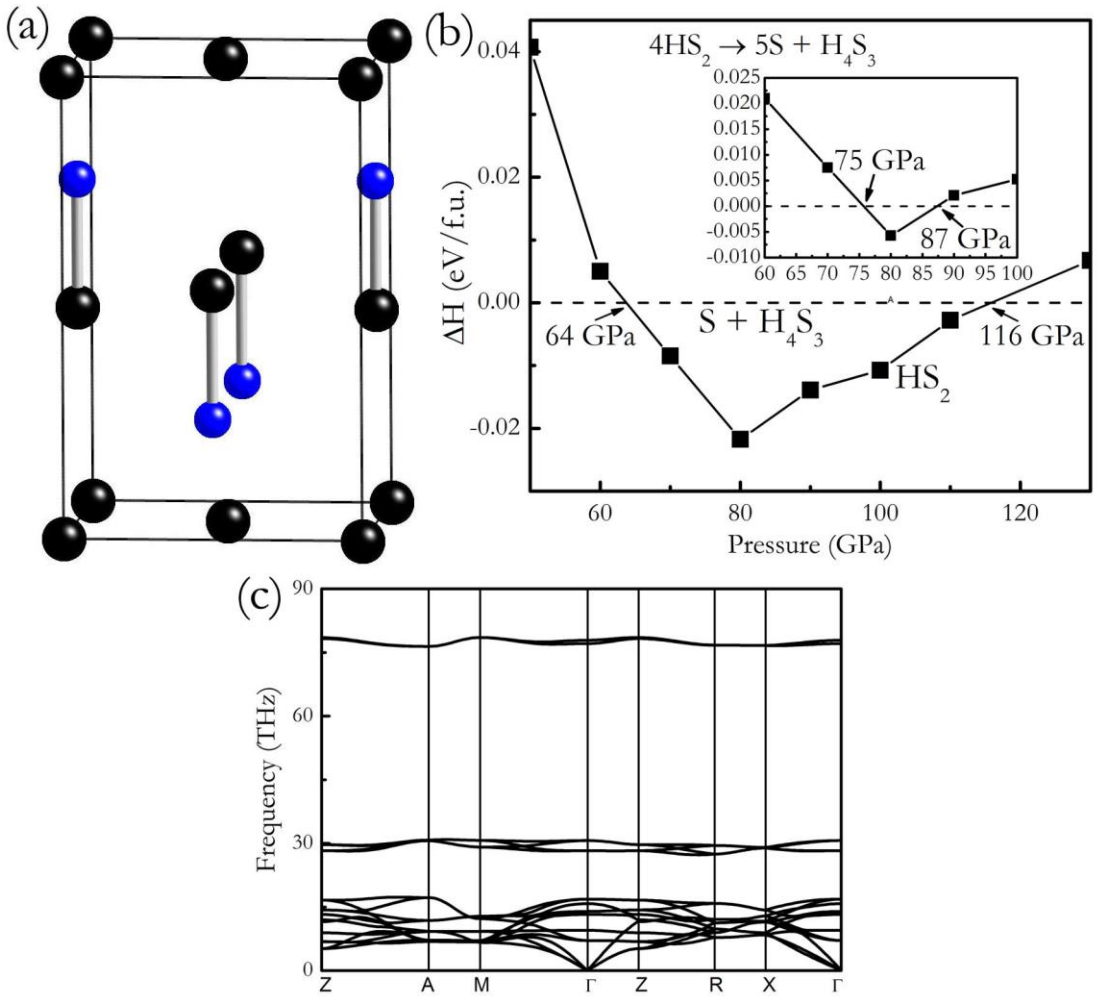

Fig. S9. (a) The predicted P4/nmm structure for HS_2 at 100 GPa. Large black and small blue spheres represent S and H atoms, respectively. (b) The static-lattice decomposition enthalpy curves of HS_2 into (H_4S_3+S) as a function of pressure. Our results show that HS_2 is energetically stable at pressures between 64 and 116 GPa on the basis of static-lattice calculations. When the zero-point vibrational enthalpy was included, the stable pressure range of HS_2 was revised to be between 75 and 87 GPa, as shown in the inset in (b). (c) Calculated phonon dispersion curve of the P4/nmm structure for HS_2 at 100 GPa, showing the dynamical stability of the structure.

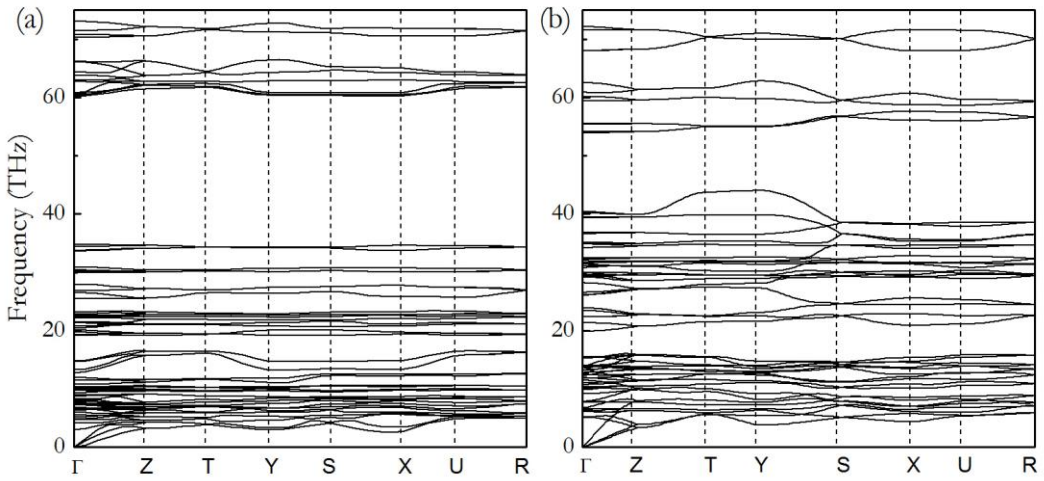

Fig. S10. (a) Calculated phonon dispersion curves of H_4S_3 in the $P2_12_12_1$ structure at 25 GPa, and (b) in the Pnma structure at 100 GPa. Both structures are dynamically stable in their corresponding stable pressure ranges.

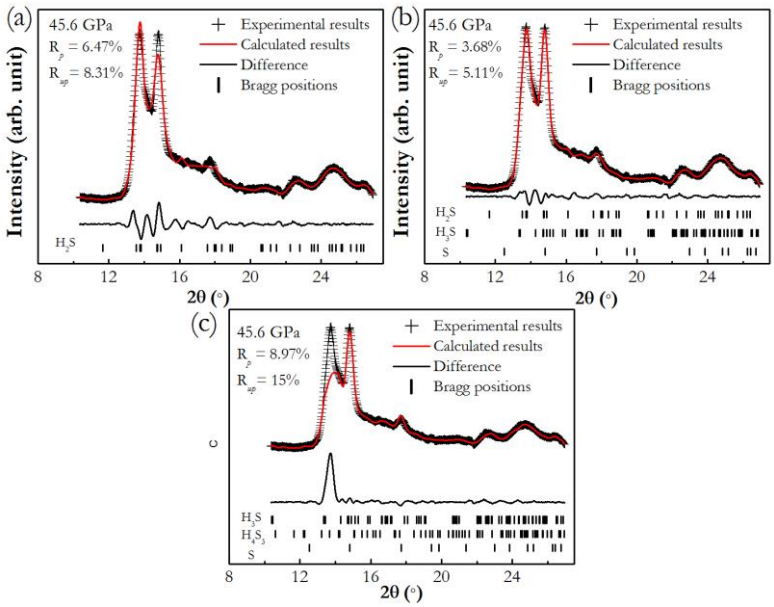

Fig. S11. Rietveld refinements of the XRD profile at 45.6 GPa based on pure H_2S (a), a mixture of H_2S + S + H_3S with phase fraction of 38:3:1 (b), and mixture of S + H_3S + H_4S_3 with phase fraction of 149:45:1. The crosses and red solid lines represent observed and fitted patterns, respectively. The solid lines at the bottom of the figures are the differences between the observed and fitted patterns. Vertical bars under the pattern represent the calculated positions of reflections arising from the compositions. The above three refinements lead to higher R_p and R_{wp} values compared to the refinement based on a mixture of H_2S + S + H_3S + H_4S_3 presented in the main text.

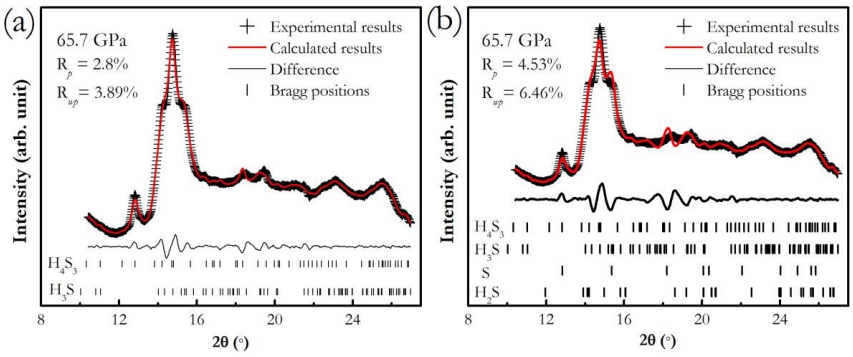

Fig. S12. Rietveld refinements of the XRD profile at 65.7 GPa based on H_4S_3 + H_3S with a phase fraction of 1.6:1 (a), or H_4S_3 + H_3S + H_2S + S with phase fraction of 13:10:3:1 (b). In (b), the phase fraction of S was fixed to 1. The crosses and red solid lines represent the observed and fitted patterns, respectively. The solid lines at the bottom of the figures are the difference between the observed and fitted patterns. Vertical bars under the pattern represent the calculated positions of reflections arising from the compositions. The above two refinements give poorer fits to the experimental data with higher R_p and R_{wp} values compared with the refinement based on a mixture of H_4S_3 + H_3S + H_2S presented in the main text.

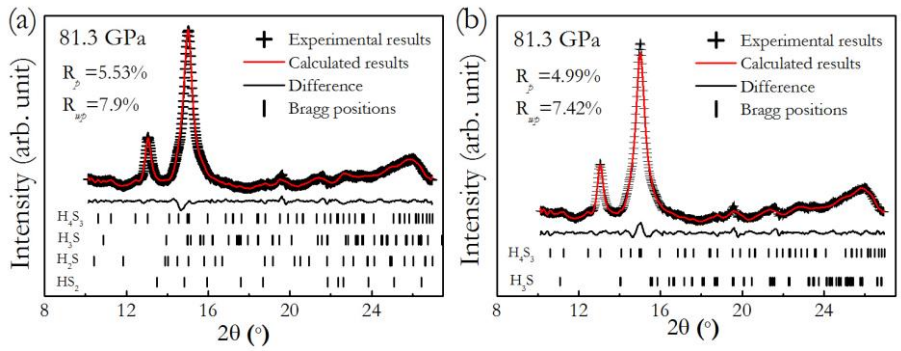

Fig. S13. Rietveld refinements of the XRD profile at 81.3 GPa based on H_4S_3 + H_3S + H_2S + HS_2 with a phase fraction of 47.4:6.6:1.1:1 (a), or H_4S_3 + H_3S with phase fraction of 12:1 (b). During the refinement, we found that the phase fraction of HS_2 is always close to zero. In (a), the phase fraction of HS_2 was constrained to 1, and the resultant larger R_{wp} and R_p values exclude HS_2 as a decomposition product.

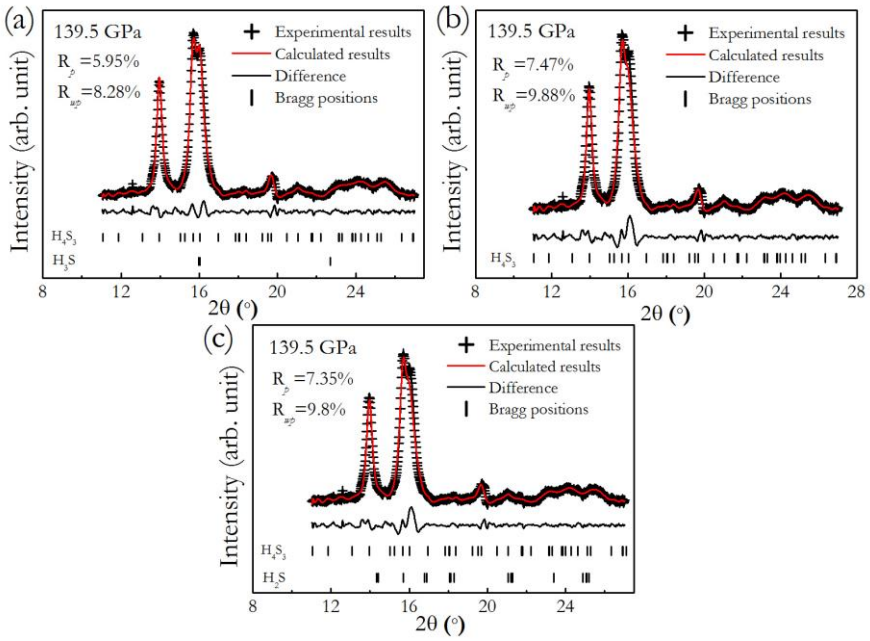

Fig. S14. Rietveld refinements of XRD profiles at 139.5 GPa based on Pnma-H_4S_3 + R3m-H_3S (a), pure Pnma-H_4S_3 (b), and Pnma-H_4S_3 + P-1-H_2S (c). Exclusion of the H_2S or H_3S or H_2S+H_3S components results in poorer fits with higher R_{wp} and R_p values than those based on H_4S_3 + H_2S + H_3S (Fig. 4 in the main text), supporting the existence of H_3S and H_2S up to 140 GPa.

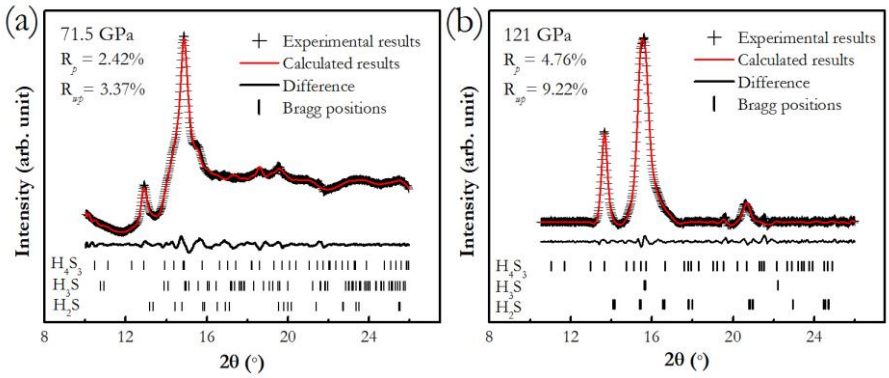

Fig. S15. Rietveld refinements of XRD profiles at 71.5 GPa based on Pnma-H_4S_3 + C2/c-H_3S + Pmc2_1-H_2S with a phase fraction of 26:5.5:1 (a), and at 121 GPa based on Pnma-H_4S_3 + R3m-H_3S + P-1-H_2S with a phase fraction of 43:5.7:1 (b).

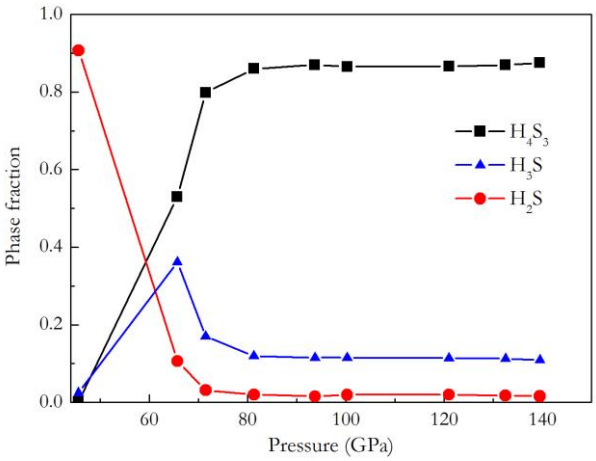

Fig. S16. Phase fraction of each component as a function of pressure. The dissociation of H_2S starts at 45.6 GPa, where its ratio begins to decrease. The phase fraction of H_3S firstly increases between 45.6 and 66 GPa because of the decomposition $8H_2S \rightarrow S + 4H_3S + H_4S_3$, and then decreases after 66 GPa due to the reaction $4H_3S + 5S \rightarrow 3H_4S_3$. Both the decomposition $8H_2S \rightarrow S + 4H_3S + H_4S_3$ and the reaction $4H_3S + 5S \rightarrow 3H_4S_3$ are related to the increasing of H_4S_3-ratio above 45.6 GPa.

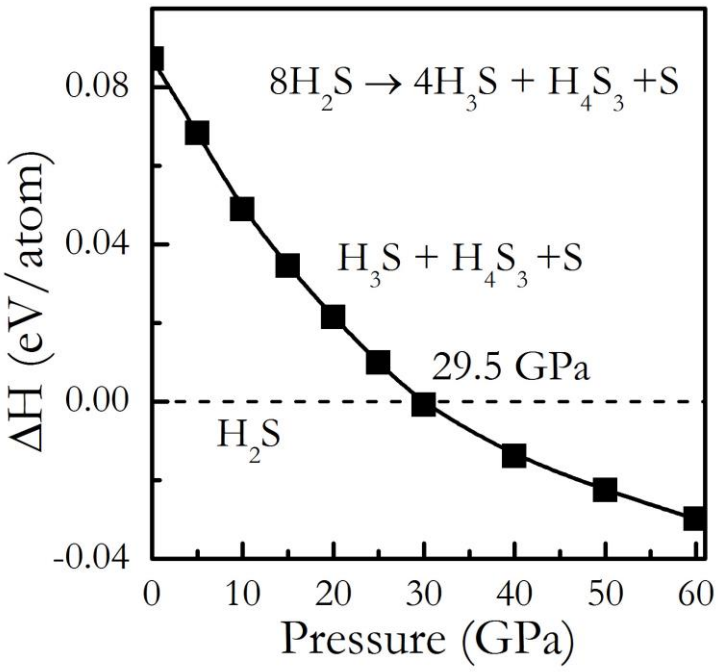

Fig. S17. Decomposition enthalpy curve of H_2S into H_3S + H_4S_3 + S as a function of pressure.

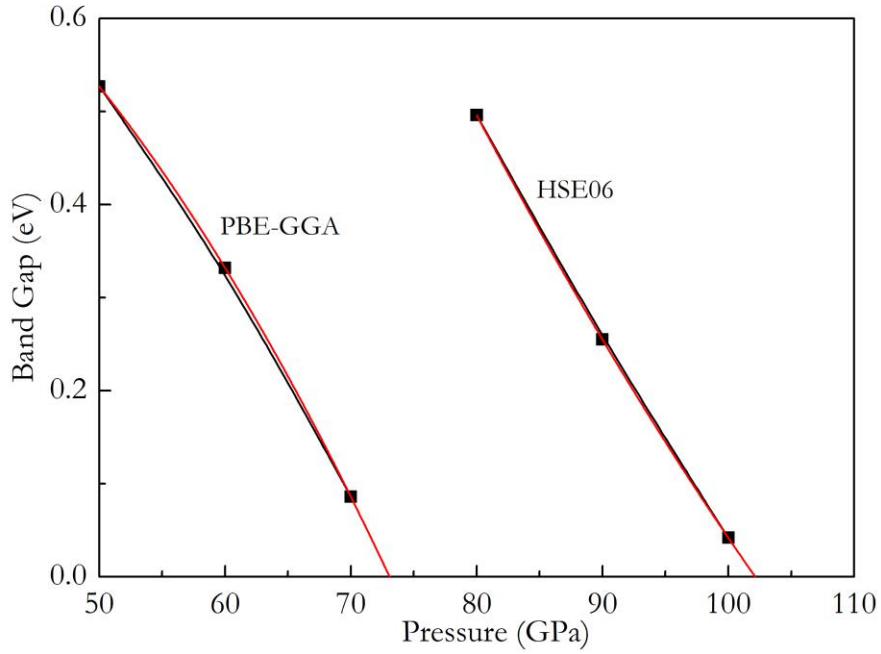

Fig. S18. Variation of band gaps with pressure for the Pnma structure of H_4S_3 calculated using the PBE-GGA functional and HSE06 hybrid functional. Our results show that H_4S_3 becomes a metal at about 102 GPa.

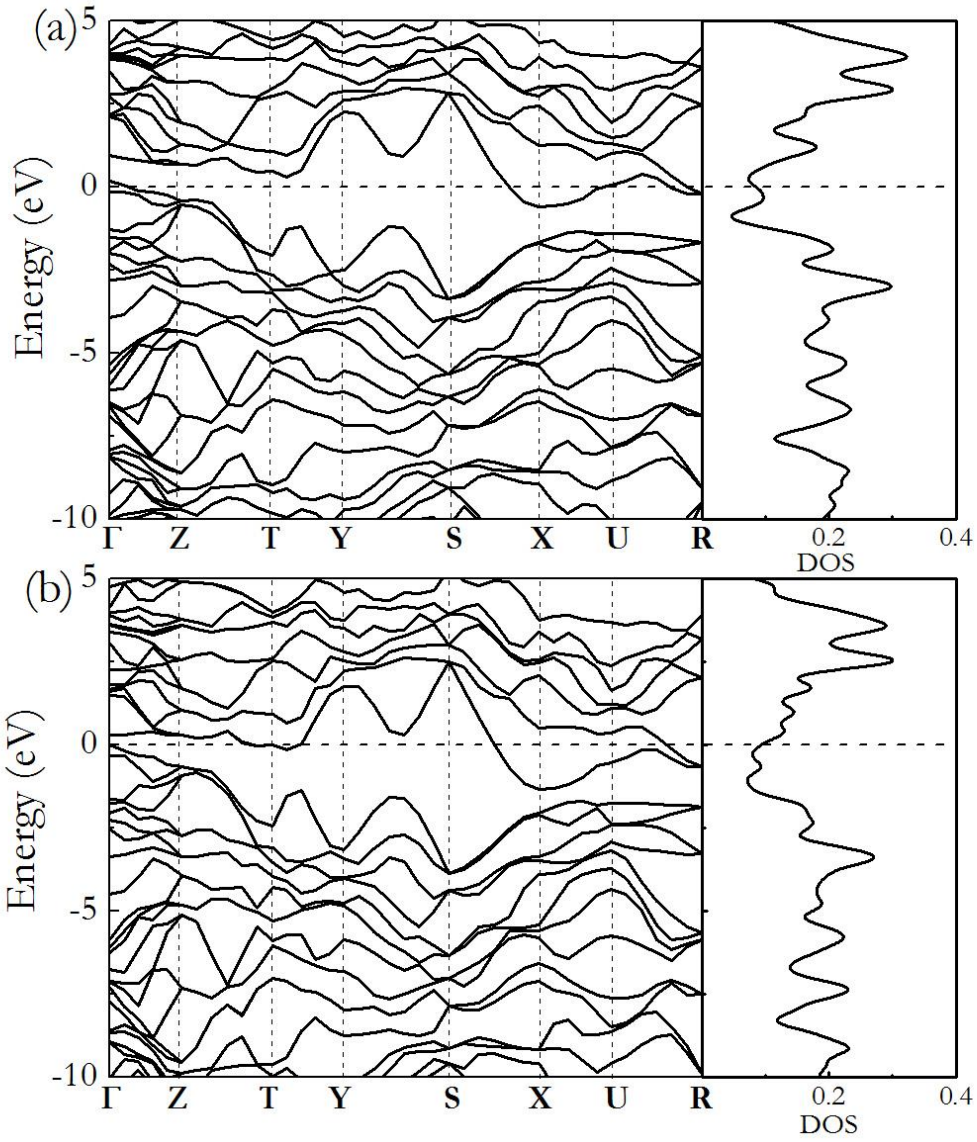

Fig. S19. Electronic band structure and density of states (DOS, in units of eV^{-1} per atom) of the Pnma structure of H_4S_3 at 110 (a) and 140 GPa (b).

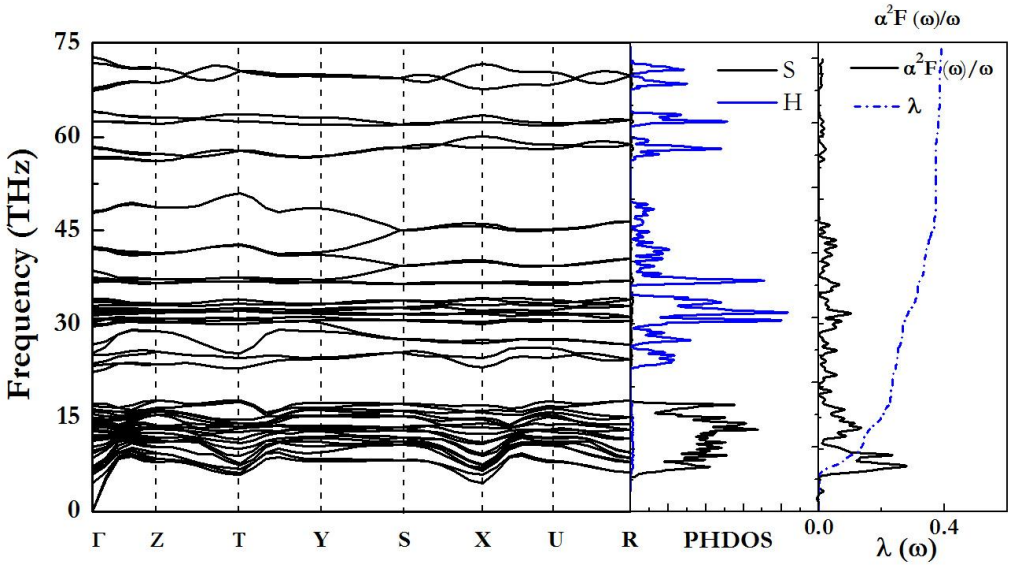

Fig. S20. Phonon dispersion curves, projected phonon density of states (PHDOS), Eliashberg spectral function $\alpha^2F(\omega)/\omega$ and EPC integration of $\lambda(\omega)$ for the Pnma structure of H_4S_3 at 140 GPa.